Talanta 88 (2012) 259–264

Contents lists available at SciVerse ScienceDirect

Talanta

journal homepage: www.elsevier.com/locate/talanta

A novel hydrogen peroxide biosensor based on the Sn–ZnNPs/MWNTs nanocomposite film

Aili Sun[a,b], Hongye Zhao[a], Jianbin Zheng[a,*]

[a] Institute of Analytical Science, Shaanxi Provincial Key Laboratory of Electroanalytical Chemistry, Northwest University, Xi'an, Shaanxi 710069, PR China
[b] Department of Chemistry and Chemical Engineering, Xinxiang University, Xinxiang 453000, PR China

ARTICLE INFO

Article history:
Received 28 June 2011
Received in revised form
13 September 2011
Accepted 15 September 2011
Available online 31 October 2011

Keywords:
Biosensor
Direct electrochemistry
Electrodeposition
Hydrogen peroxide
Sn–ZnNPs

ABSTRACT

The Zn–Sn nanoparticles/multiwall carbon nanotubes (Zn–SnNPs/MWNTs) nanocomposite film was prepared by electrodeposition of $ZnCl_2$ and $SnCl_2$ on MWNTs simultaneously in Ethaline ionic liquids. Then, based on immobilizing hemoglobin (Hb) within a novel Zn–SnNPs/MWNTs nanocomposite film (Hb/Zn–SnNPs/MWNTs), a novel hydrogen peroxide (H_2O_2) biosensor was constructed. Meantime, the morphology of the Zn–SnNPs and analytical characteristics of the biosensor were investigated. A high density and well-distributed Zn–SnNPs spheres with an average diameter of 120 nm was observed by field emission scanning electron microscopy. The voltammetric results of the biosensor showed a pair of well-defined and quasi-reversible redox peaks of Hb with a formal potential ($E^{0'}$) of −0.40 V and a peak-to-peak separation (ΔE_p) of 0.086 V. Moreover, the biosensor exhibited an excellent electrocatalytic activity to H_2O_2 with a K_M value of 0.379 mM; the reduction peak currents of Hb on the Hb/Zn–SnNPs/MWNTs/GCE were linearly related to H_2O_2 in the range from 0.5 to 840 μM with a correlation coefficient of 0.9984 and a detection limit of 0.11 μM (S/N = 3). Results demonstrated that Zn–SnNPs/MWNTs nanocomposite film was promising a new platform for the construction of H_2O_2 biosensors and provided a way to develop other biologic active materials in ionic liquids.

1. Introduction

In recent years, room temperature ionic liquids (RTILs) have attracted much attention in the fields of electroanalysis and electrochemistry. The electrodeposition of pure metals or alloys from ionic liquids (ILs) has received significant interest [1–7], based on such electrodeposition in ionic liquid, many of metal and alloy-coated electrodes have been developed for nonenzymatic electrochemical determination [6]. Reports showed that composite films synthesized in ILs possessed superior properties of significantly enhanced electrochemical activity, greater conductivity, and superior mechanical behavior [7].

Nowadays, great interests have been focused on nanoparticles [8–12] in biosensor field since it can offer many advantages, such as large high surface reaction activity and strong adsorption ability to immobilize the desired biomolecules [13–15]. Meanwhile, bimetallic alloys nanoparticles have been widely used in catalysis and sensing fields, due to their unique properties different from those of the bulk materials [16–18]. However, few reports were concerned with direct electron transfer of proteins or enzymes at Zn, Sn and Zn–Sn nanoparticles (Zn–SnNPs) films, even Zn and Sn are much cheaper. For the electrodeposition of active metals, hydrogen evolution is not preventable in aqueous solutions [6].

In this paper, we firstly proposed the application of Sn–ZnNPs in the bioelectrochemistry to realize direct electron transfer of hemoglobin (Hb). Electrodeposition of Zn–SnNPs in ILs on the substance of multi-wall carbon nanotubes (MWNTs) was realized to exploit their synergistic contributions on the improvement of biosensor characteristics. Using Hb as a model protein, the constructed biosensor displayed a fast electron transfer and a good electrochemical activity for the detection of hydrogen peroxide (H_2O_2), with wide linear range and low detection limit. Therefore, the present work offers a new avenue to broaden the applications of Sn–ZnNPs in electrochemical biosensors.

2. Experimental

2.1. Reagent and materials

Bovine hemoglobin (Hb, MW 64,500) was purchased from Sigma (St. Louis, USA). The MWNTs (>95% purity) were purchased from Chengdu Organic Chemicals Co. Ltd., of the Chinese Academy of Science. Chitosan (CS, MW 5–6 × 10^5, >90% deacetylation) was purchased from Shanghai Yuanju Biotechnology Co. Ltd. (Shanghai

* Corresponding author. Tel.: +86 29 88302077; fax: +86 29 88303448.
E-mail address: zhengjb@nwu.edu.cn (J. Zheng).

0039-9140/$ – see front matter © 2011 Elsevier B.V. All rights reserved.
doi:10.1016/j.talanta.2011.09.067

Yuanju, China). H_2O_2 (w/w, 30%) was obtained from Tianjin Tianli Chemistry Reagent Co. Ltd. (Tianjin, China,). 0.1 M phosphate buffer saline (PBS) was used as the supporting electrolyte. All other reagents and chemicals were of analytical reagent grade and doubly distilled water was used in experiments.

All the electrochemical experiments were carried out on a CHI660D electrochemical workstation (Shanghai Chenhua Instrument Co. Ltd., China) using a three electrode system, where a standard saturated calomel electrode (SCE) served as reference electrode, a platinum wire electrode as the auxiliary electrode, and the modified electrodes glassy carbon electrode (GCE) as the working electrode. All the potentials given in this paper were referred to the SCE. Field emission scanning electron microscopy (FE-SEM) and energy dispersive spectrometer (EDS) images were acquired with a JEOL JEM-6700 (JEOL, Japan) using an accelerating voltage of 200 kV. FT-IR spectra were obtained on a Tensor 27 FT-IR spectrophotometer (Bruker Company, Germany). All the tested solutions were purged with highly purified nitrogen for 30 min before the experiments and a nitrogen environment was kept over the solution during the electrochemical measurements. All electrochemical experiments were conducted at room temperature ($25 \pm 2\,^{\circ}C$).

2.2. Preparation of ionic liquids and electrodeposition of bimetallic alloys nanoparticles

The ionic liquids Ethaline were synthesized according to Ref. [19]. Briefly, ethylene glycol and choline chloride (2:1) was heated by continuous stirring until a homogeneous, colorless liquid was formed. Cyclic voltammetry was employed for the electrodeposition of Sn–ZnNPs onto the prepared MWNTs/GCE with the mixture solution of 0.5 M $ZnCl_2$ and 0.05 M $SnCl_2$. The potential range for multiple cyclic voltammetric experiments was from 1.2 to −0.8 V (vs SCE) with a scan rate of 20 mV/s. The fabricated Sn–ZnNPs modified MWNTs/GCE (Sn–ZnNPs/MWNTs/GCE) was rinsed by double-distilled water and dried in air for further use. For comparison, ZnNPs/MWNTs/GCE and SnNPs/MWNTs/GCE were prepared with the same procedure.

2.3. Preparation of Hb/Zn–SnNPs/MWNTs

The GC electrode (Ø = 4 mm) was polished with 0.3 and 0.05 μm alumina slurry to obtain mirror like surface, and ultrasonically cleaned in ethanol and water thoroughly. Then it was allowed to dry at room temperature. 2 mg of the acid-treated MWNTs was ultrasonically dispersed in 2 mL of CS solution (1 wt.%) to obtain a homogeneous black suspension of 1.0 mg/mL. Subsequently, the MWNTs film was prepared by dropping 8 μL of this black suspension on a cleaned GC electrode surface and then drying slowly in air at room temperature. After that, Sn–ZnNPs was electrodeposited from IL and dried in air to obtain Sn–ZnNPs/MWNTs nanocomposite film. At last, 8 mg of Hb was dissolved in 1 mL of CS solution (1 wt.%) and hand-mixed completely, 8 μL of the mixture was added into the Sn–ZnNPs/MWNTs/GCE for the construction of H_2O_2 biosensors. A beaker was covered over the electrode so that water could evaporate slowly. The preparation process of modified electrode was shown in Scheme 1. The modified electrodes were stored in a refrigerator (4 °C) until further use.

3. Results and discussion

3.1. Electrodeposition and characterize of Sn–ZnNPs

Fig. 1A showed the cyclic voltammograms (CVs) of $ZnCl_2$ and $SnCl_2$ in IL. Two cathodic peaks with the peak potential of −1.063 V

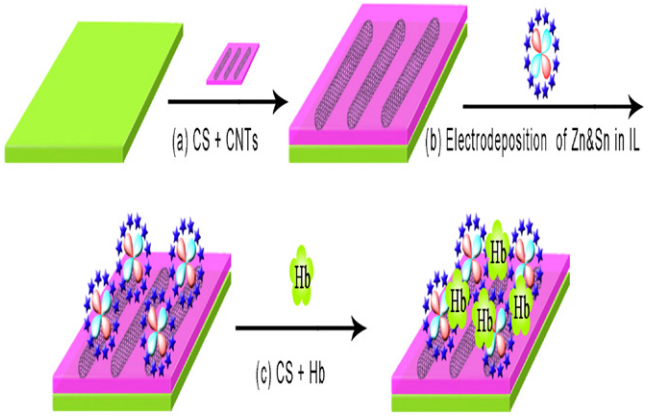

Scheme 1. The illustration of the preparation process of modified electrode.

(peak a) and −0.679 V (peak b) could be ascribed to the reduction of Sn^{2+} and Zn^{2+}, respectively. However, when a mixture of $ZnCl_2$ and $SnCl_2$ was electrodeposited under the same condition, two cathodic peaks located at −1.178 V and −0.639 V was observed (Fig. 1B), which was demonstrated that Sn–Zn alloys nanoparticles was deposited on the surface of electrode successfully.

3.2. FE-SEM and EDS measurements of Sn–ZnNPs/MWNTs nanocomposite film

The structural and morphological characters of Sn–ZnNPs coated MWNTs nanocomposite film were obtained by FE-SEM

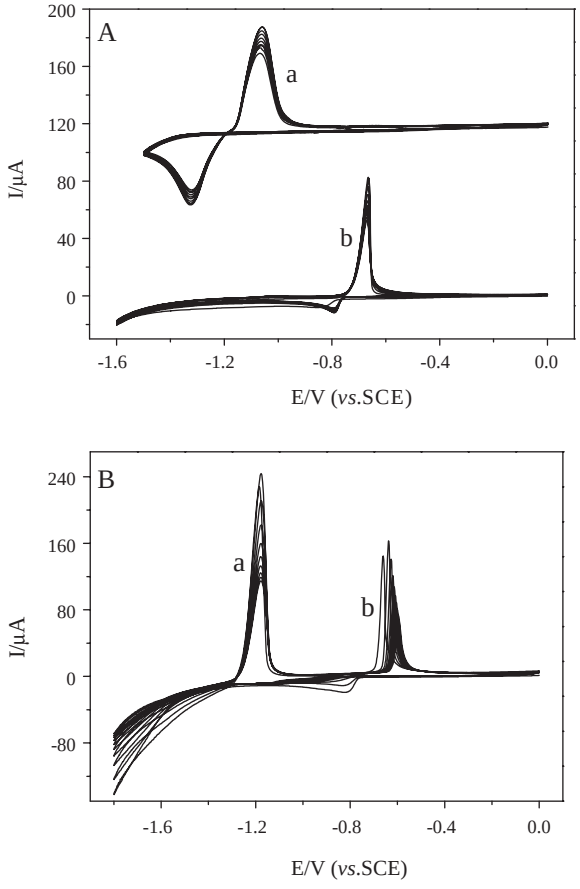

Fig. 1. (A) CVs recorded at GCE in Ethaline ionic liquid containing 0.05 M $SnCl_2$ (a), 0.50 M $ZnCl_2$ (b), and (B) a mixture combined 0.50 M $ZnCl_2$ with 0.05 M $SnCl_2$. Scan rate: 0.02 V s^{-1}.

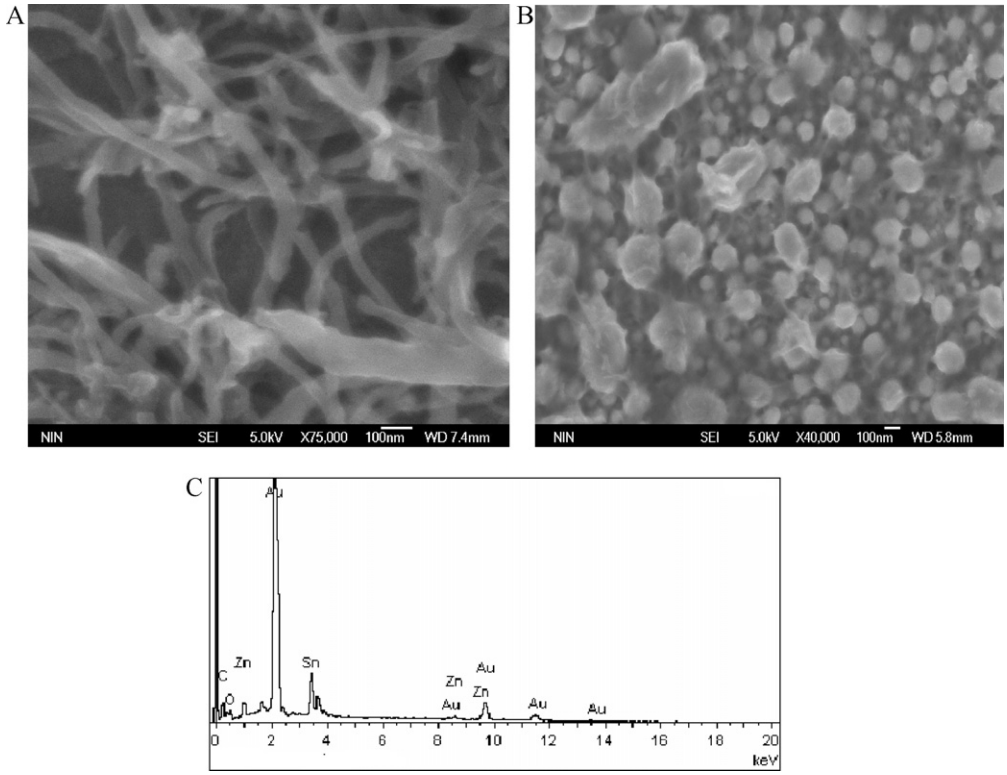

Fig. 2. FE-SEM micrographs of MWNTs (A) and Sn–ZnNPs coated MWNTs (B), EDS analysis of Sn–ZnNPs coated MWNTs nanocomposite film (C).

analysis. The MWNTs displayed dispersed well and the diameter of MWNTs spanned from 30 to 50 nm (in Fig. 2A). Many Sn–ZnNPs could be observed with an average diameter of 120 nm on the surface of MWNTs, which indicated that Sn–ZnNPs had been deposited on the surface of MWNTs homogeneously with high density and well-distribution (in Fig. 2B). The EDS spectrum (Fig. 2C) showed the presence of Zn and Sn with an atomic ratio of 1:8. The results demonstrated that Sn–ZnNPs were successfully electrodeposited on MWNTs.

3.3. FT-IR characterization of Sn–ZnNPs/MWNTs nanocomposites film

FT-IR spectroscopy is an effective means to explore the secondary structure of proteins [20]. The characteristic amide I and II bands of proteins provide detailed information of the secondary structure of polypeptide chain. The amide I band (1700–1600 cm^{-1}) is attributed to the C=O stretching vibrations of peptide linkages in the backbone of the protein. The amide II band (1600–1500 cm^{-1}) is attributed to the combination of N–H bending and C–N stretching of the peptide groups [21]. FT-IR spectrum of the Hb/Sn–ZnNPs/MWNTs nanocomposite film (Fig. 3, curve b) displayed a peak at 1643 cm^{-1} and another at 1550 cm^{-1}, and had similar shapes to that of the native Hb (Fig. 3, curve a), which exhibited two strong peaks at 1652 cm^{-1} and 1556 cm^{-1}. The results suggested that Hb well retained the essential feature of its secondary structure after immobilized in the Sn–ZnNPs/MWNTs nanocomposite film. As a result, Sn–ZnNPs/MWNTs nanocomposite film may provide a promising matrix for enzyme immobilization because of its satisfying biocompatibility.

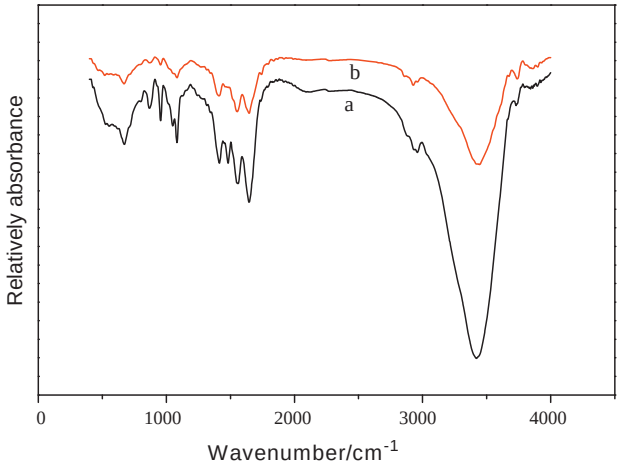

Fig. 3. FT-IR spectra of (a) Hb and (b) Hb/ZnSnNPs/MWNTs films.

3.4. Electrochemical characteristics of Hb at the Zn–SnNPs/MWNTs nanocomposite film

Fig. 4 shows the CVs of different modified electrodes in pH 7.0 PBS at a scan rate of 0.10 V s^{-1}. No redox peaks were observed at the bare GCE (curve a), MWNTs/GCE (curve b) and Zn–SnNPs/MWNTs/GCE (curve d), which indicated that no electroactive substances existed on the electrode surface. The CVs of the Hb/MWNTs/GCE (curve c), Hb/ZnNPs/MWNTs/GCE (curve e) and Hb/SnNPs/MWNTs/GCE (curve f) showed that only a small reduction peak appeared, indicating the direct electron transfer of Hb was not realized. On the Hb/Zn–SnNPs/MWNTs/GCE, the electrochemical responses increased (curve g), and a pair of well-defined quasi-reversible redox peaks appeared. From the CV of Hb/Zn–SnNPs/MWCNTs/GCE, the values of E_{pa} and E_{pc} were obtained at −0.444 V and −0.358 V (vs SCE), respectively, with the ratio of the redox peak currents as a unity. The formal potential ($E^{0'}$), which was defined as the average value of the anodic and cathodic peak potential with the equation as $(E^{0'}) = (E_{pa} + E_{pc})/2$,

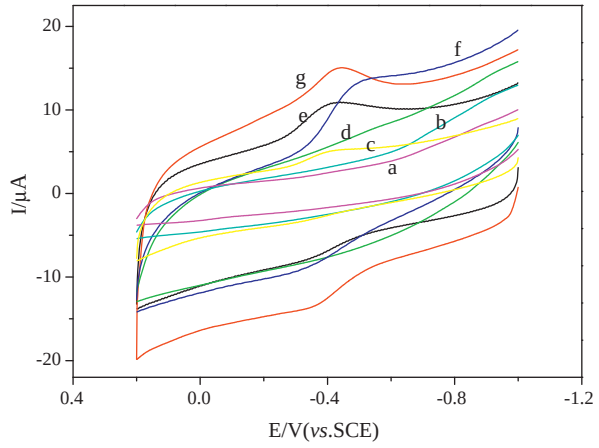

Fig. 4. CVs of bare GCE (a), MWNTs/GCE (b), Hb/MWNTs/GCE (c), Zn–SnNPs/MWNTs/GCE (d), Hb/ZnNPs/MWNTs/GCE (e), Hb/SnNPs/MWNTs/GCE (f), Hb/ZnSnNPs/MWNTs/GCE (g) in pH 7.0 PBS at a scan rate of 0.10 V s^{-1}.

was calculated as −0.401 V (vs SCE), The peak-to-peak separation was about 0.086 V at the scan rate of 0.10 V s^{-1}. All of the above results revealed that the presence of Zn–SnNPs showed improvement to the direct electron transfer rate of Hb. The combination of Zn–SnNPs with MWNTs nanocomposite film provided a high metal conductivity and increased surface area, which promoted the electron transport efficiency and facilitated the direct electron transfer of Hb.

The influence of the scan rate on the electrochemical response of Hb/Zn–SnNPs/MWNTs/GCE was further investigated, and the results were shown in Fig. 5. With an increasing scan rate, the redox potentials (E_{pa} and E_{pc}) of Hb hardly shift. Moreover, both the cathodic and anodic peak currents increased linearly with the scan rates (v) in a range from 0.08 to 1.50 V s^{-1}. The linear regression equation was I_{pa} (μA) = −1.389 − 22.17v (V s^{-1}) (n = 16, r = 0.9990) and I_{pc} (μA) = 2.706 + 23.79v (V s^{-1}) (n = 16, r = 0.9991). Such results indicated that the electrochemical kinetics was a diffusion-controlled process. According to the equation of $I_p = n^2F^2vA\Gamma/4RT = nFQv/4RT$. n was calculated as 0.93, meaning that one electron transfer was involved. Meantime, according to the

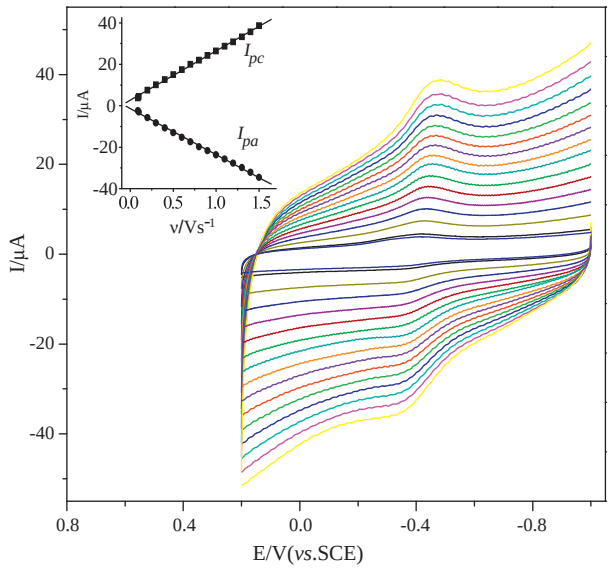

Fig. 5. CVs of Hb/ZnSnNPs/MWNTs/GCE in pH 7.0 PBS with different scan rates (from a to n): 0.08, 0.10, 0.20, 0.30, 0.40, 0.50, 0.60, 0.70, 0.80, 0.90, 1.00, 1.10, 1.20, 1.30, 1.40, 1.50 V s^{-1}.

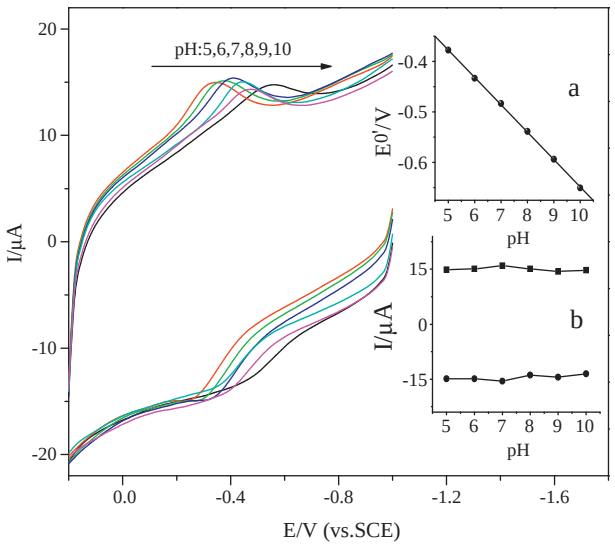

Fig. 6. Influence of pH value on CVs of Hb/Sn–ZnNPS/MWNTs/GCE pH values (from left to right): 5.0, 6.0, 7.0,8.0, 9.0, 10.0. Inset: the relationship between $E^{0'}$ and pH values. Scan rate: 0.1 V s^{-1}.

Laviron's equation [22]: $\Gamma^* = Q/nFA$, the charge values (Q) were nearly constant at different scan rates, and the average value of Γ^* was calculated as 3.93×10^{-10} mol cm^{-2}, which was much higher than the value of monolayer protein (1.89×10^{-11} mol cm^{-2}) on the electrode surface [23]. The reason may be that the presence of Zn–SnNPs could provide an increased surface area for Hb immobilization. The electron transfer rate constant (k_s) of Hb on the modified electrode could be obtained by the following equation [24]:

$$\log k_s = \frac{\alpha \log(1-\alpha) + (1-\alpha)\log \alpha - \log(RT/nFv) - (1-\alpha)\alpha F\Delta E_p}{2.3RT}$$

where α is the charge transfer coefficient, and n is the number of electron transfer. R, T and F have their conventional meanings. ΔE_p is the peak-to-peak potential separation. On the basis of the relationship of E_p vs log v, the values of electron transfer coefficient (α) was calculated as 0.48, the value of k_s was estimated to be 0.86 s^{-1}, the value of electron transfer rate constants of Hb/MWNTs, Hb/Sn/MWNTs, and Hb/Zn/MWNTs was estimated to 0.42 s^{-1}, 0.69 s^{-1}, 0.52 s^{-1}, respectively in this paper, which was larger than that of Hb immobilized on carbon nanotube of 0.49 s^{-1} [25] and Co/CILE 0.588 s^{-1} [26].

3.5. Influence of pH value

In order to obtain optimal conditions for the determination of H_2O_2, the influence of pH value on the direct electrochemistry of the Hb/Sn–ZnNPS/MWNTs/GCE was recorded in Fig. 6. With the increase of pH value from 5.0 to 10.0, the cathodic peak currents increased and reached a maximum at around pH 7.0 and then decreased with further increased pH value. Thus, the optimal pH value of the biosensor was selected at pH 7.0. The linear regression equation was obtained as $E^{0'}$ (mV) = −0.081 − 0.042 pH (n = 6, r = 0.9999) (inset of Fig. 6. The slope value of 42.00 mV/pH was smaller than the theoretically expected value of 59 mV/pH at 25 °C for a single-proton coupled reversible one-electron transfer [27]. The reason might be the influence of the protonation states of trans-ligands to the heme iron and amino acids around the heme, or the protonation of the water molecule coordinated to the central iron

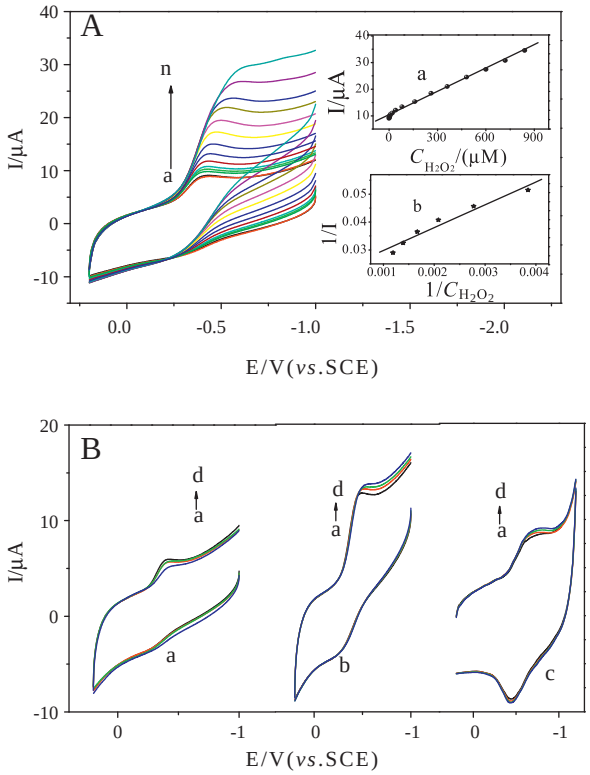

Fig. 7. (A) CVs of Hb/Sn–ZnNPs/MWNTs/GCE in the presence of a–n in the presence of 0, 0.5, 1.5, 2.5, 5, 10, 20, 40, 80, 160, 260, 360, 480, 600, 720, 840 μM H_2O_2, respectively. Inset: relationship of the catalytic peak current and the concentration of H_2O_2 (a) and the linear part of the calibration curve (b), and (B) CVs of Hb/MWNTs/GCE (a), Hb/SnNPs/MWNTs/GCE (b), Hb/ZnNPs/MWNTs/GCE (c) in the presence of (a–d) 0, 20.0, 40.0, 80.0 μM H_2O_2 H_2O_2. Scan rate: 0.10 V s^{-1}.

[28]. But the electron-transfer between Hb and the electrode could also be represented as [29]

$$\text{Hb Fe(III)} + \text{H}^+ + \text{e}^- \leftrightarrow \text{Hb Fe(II)}$$

3.6. Electrocatalysis of Hb to H_2O_2

The electrocatalytic activity of the Hb/Zn–SnNPs/MWNTs/GCE toward H_2O_2 was investigated by CV. As shown in Fig. 7, with the addition of H_2O_2, the cathodic peak current at −0.436 V was increased greatly while the anodic peak current gradually disappeared, which demonstrated the typical electrocatalytic reduction process of H_2O_2. The catalytic reduction peak was proportional to the H_2O_2 concentration in the range from 0.5 to 840 μM (Fig. 7, inset), and the linear regression equation was I_p (μA) = 10.45 + 2.9 × 10^{-2} C (μM) (n = 16, r = 0.9984) with a detection limit of 0.11 μM (S/N = 3) and the sensitivity was 29.2 μA mM^{-1}. When the concentration of H_2O_2 was more than 840 μM, a response plateau was observed, showing a typical Michaelis–Menten kinetic mechanism. The apparent Michaelis–Menten constant (K_M) could be calculated by the Lineweaver-Burk equation [30]:

$$\frac{1}{I_{ss}} = \frac{1}{I_{max}} + \frac{K_M}{I_{max}C}$$

Here I_{ss} is the steady-state current after the addition of the substrate, C is the bulk concentration of the substrate, and I_{max} is the maximum current measured under the saturate substrate conditions. The value of K_M and I_{max} could be obtained by the slope and the intercept of the plot of the reciprocals of the steady-state current vs H_2O_2 concentration. On the basis of the experimental data, the K_M value was calculated as 0.379 mM, which was lower than the reported values of 1.3 mM [31] and 85.7 mM [32]. The result showed that the immobilized Hb in the Zn–SnNPs/MWNTs nanocomposite film modified electrode had a higher biological affinity to H_2O_2. The possible mechanism of electrocatalytic reduction of H_2O_2 at Hb-based electrode has been reported [33]:

$$\text{Hb[Heme(Fe(III))]} + \text{H}_2\text{O}_2 \rightarrow \text{CompoundI} + \text{H}_2\text{O} \quad (1)$$

$$\text{CompoundI} + \text{H}_2\text{O}_2 \rightarrow \text{Hb[Heme(Fe(III))]} + \text{H}_2\text{O} + \text{O}_2 \quad (2)$$

$$\text{Hb[Heme(Fe(III))]} + \text{H}^+ + \text{e}^- \rightarrow \text{Hb[Heme(Fe(II))] at electrode} \quad (3)$$

$$\text{Hb[Heme(Fe(II))]} + \text{O}_2 \rightarrow \text{Hb[Heme(Fe(II))]} - \text{O}_2 \text{ fast} \quad (4)$$

$$\text{Hb[Heme(Fe(II))]} - \text{O}_2 + \text{H}^+ + \text{e}^- \rightarrow \text{Hb[Heme(Fe(III))]} + H_2O_2 \text{ at electrode} \quad (5)$$

The overall reaction of (1)–(5) would be:

$$\text{H}_2\text{O}_2 + 2\text{H}^+ + 2\text{e}^- \rightarrow 2\text{H}_2\text{O} \quad (6)$$

For comparison, the electrocatalytic activity of the Hb/MWNTs/GCE, the Hb/SnNPs/MWNTs/GCE, and the Hb/ZnNPs/MWNTs/GCE (Fig. 7B, a–c), toward different concentrations of H_2O_2 was also investigated, respectively. It was found that the electrode only modified with MWNTs, SnNPs/MWNTs or ZnNPs/MWNTs showed a detectable but a relatively small current response to H_2O_2. These results demonstrated that the Zn–SnNPs exhibited a better catalytic property than did their monometallic counterparts of ZnNPs and SnNPs, due to the synergistic effect of the Zn–SnNPs.

In order to assess the analytical performance level of the proposed biosensor, the characteristics of the proposed biosensor were compared with other H_2O_2 biosensors [34–40] as shown in Table 1.

Results showed that the linearity range, detection limit and the value of K_M of the proposed biosensor were better than previously reported models. The favorable performances of the biosensor were attributed to the excellent conductivity and biocompatibility of Zn–SnNPs/MWNTs nanocomposite film. Meanwhile, there is a synergistic activity among Zn–SnNPs and MWNTs.

3.7. Repeatability and stability of the biosensor

The repeatability of the measurement was obtained by ten parallel determinations of 0.05 mM H_2O_2 using the same electrode. The relative standard deviation (R.S.D.) was found to be 3.6%. To evaluate the electrode-to-electrode reproducibility, five electrodes were prepared under the same conditions independently. The result revealed a R.S.D. of 4.2%, indicating an acceptable reproducibility.

Meantime, electrode stability was tested every two days. And it could maintain 88.2% of its initial electrochemical response after two weeks, demonstrating good long-term stability. The good long-term stability could be attributed to the good biocompatibility of the composites, and could provide a favorable microenvironment for Hb to retain its bioactivity.

3.8. Selectivity against interferences

The influence of some possible interfering substances were examined to evaluate the selectivity of this H_2O_2 biosensor, when the concentration of interfering substances was 0.15 mM AA, 5.0 mM glucose and 0.5 mM UA, it caused a decrease of 1.2%, 2.6% and 3.8% in the reduction current of 1.0 mM H_2O_2. It can be concluded that the three tested interferents exerted neglectable influences on the determination of H_2O_2.

Table 1
Performances of different H_2O_2 biosensors.

Biosensor	LR[a] (μM)	DL[b] (μM)	K_M (mM)	Reference
Hb-C@Au/GCE	5–135	1.67	88.6	[34]
Hb/PCNFs/BMIM·PF6/CHIT	2.0–440	0.70	10.2	[35]
Nafion/Hb/Au/CILE	200–18,000	160	0.499	[36]
Hb/MWNT/GCE	6–600	1.2	–	[37]
PVA/Hb/MWCNTs/CILE	1.2–30.0	1.0	0.928	[38]
Hb/SA-MWCNTs/GCE	40–200	16.41	0.533	[39]
Hb/ZnO-MWCNTs/Nafion	0.2–12	0.08	82.2	[40]
Hb/Zn–SnNPs/MWNTs/GCE	0.5–840	0.11	0.379	This work

[a] Linear range.
[b] Detection limit.

Table 2
Detection results of H_2O_2 in disinfector sample.

Sample	This method (mol L^{-1})	RSD (%)	$KMnO_4$ titration method (mol L^{-1})	RSD (%)
1	2.73×10^{-4}	4.3	3.21×10^{-4}	3.5
2	4.60×10^{-5}	3.2	4.89×10^{-5}	2.8
3	5.2×10^{-6}	3.6	5.43×10^{-6}	2.5

3.9. H_2O_2 determination in real sample

In order to investigate the reliability of the H_2O_2 biosensor, the concentrations of H_2O_2 in disinfectant samples were measured using the method proposed above and the traditional method detected by $KMnO_4$. The determination results were summarized in Table 2. It can be seen that the results obtained using the proposed method were consistent with the KMnO4 titration method. The results were in acceptable agreement and the proposed sensor can be used in the determination of H_2O_2 in real samples.

4. Conclusions

In summary, Zn–SnNPs were successfully prepared by the electrodeposition in the ionic liquid Ethaline supported on MWNTs modified electrode. The nanocomposite containing Zn–SnNPs and MWNTs was successfully applied to fabricate the biosensor for the first time. Electrochemical studies showed that fast direct electron transfer of Hb was obtained between Zn–SnNPs/MWNTs nanocomposite film modified GCE and Hb, and a highly catalytic activity to H_2O_2. Compared with other H_2O_2 biosensors showed in Table 1, the proposed biosensor has advantages of low detection limit and wide linear range. The reason might be that Zn–SnNPs which electrodeposition in the ionic liquid not only provides a suitable environment for Hb to retain the native structure, but also established efficient electronic communication between proteins and the electrode. Thus the present biosensor provided a good electrochemical sensing platform for redox proteins and application in biosensors and biocatalysis.

Acknowledgements

The authors appreciate the financial support from the National Natural Science Foundation of China (No. 20875076), the Education Department of Shaanxi Province, China (No. 2010JK877), the Natural Science Foundation of Henan Province (No. 102300410185) and Science and Technology innovation Foundation of XinXiang University.

References

[1] H.Y. Huang, P.Y. Chen, Electrochim. Acta 56 (2011) 2336–2343.
[2] P.Y. Chen, M.J. Deng, D.X. Zhuang, Electrochim. Acta 54 (2009) 6935–6940.
[3] F.Q. Zhao, F. Xiao, B.Z. Zeng, Electrochem. Commun. 12 (2010) 168–171.
[4] M.J. Deng, P.Y. Chen, T.I. Leong, I.W. Sun, J.K. Chang, W.T. Tsai, Electrochem. Commun. 10 (2008) 213–216.
[5] S. Legeai, S. Diliberto, N. Stein, C. Boulanger, J. Estager, N. Papaiconomou, M. Draye, Electrochem. Commun. 10 (2008) 1661–1664.
[6] H.Y. Huang, P.Y. Chen, Talanta 83 (2010) 379–385.
[7] Q. Wang, Y.B. Yun, J.B. Zheng, Microchim. Acta 167 (2009) 153–157.
[8] D. Vennerberg, Z.Q. Lin, Sci. Adv. Mater. 3 (2011) 26–40.
[9] S. Shiv Shankar, Sasanka Deka, Sci. Adv. Mater. 3 (2011) 169–195.
[10] H. Jeong, M.S. Ahmed, S. Jeon, J. Nanosci. Nanotechnol. 11 (2011) 987–993.
[11] D. Narducci, Sci. Adv. Mater. 3 (2011) 426–435.
[12] R.R. Zhuang, F.F. Jian, K.F. Wang, Sci. Adv. Mater. 2 (2010) 151–156.
[13] W.Y. Cai, Q. Xu, X.N. Zhao, J.J. Zhu, H.Y. Chen, Chem. Mater. 18 (2006) 279–284.
[14] L.Q. Yang, X.L. Ren, F.Q. Tang, L. Zhang, Biosens. Bioelectron. 25 (2009) 889–895.
[15] A.J. Saleh Ahammad, S. Sarker, J.J. Lee, J. Nanosci. Nanotechnol. 11 (2011) 5670–5675.
[16] X.Y. Pang, D.M. He, S.L. Luo, Q.Y. Cai, Sens. Actuators B 137 (2009) 134–138.
[17] D. Jana, A. Dandapat, G. De, J. Phys. Chem. C 113 (2009) 9101–9107.
[18] J. Yang, L.C. Jiang, W.D. Zhang, S. Gunasekaran, Talanta 82 (2010) 25–33.
[19] A.P. Abbott, J.C. Barron, K.S. Ryder, Trans. Inst. Met. Finish. 87 (2009) 201–207.
[20] L. Gao, Q. Gao, Q. Wang, S. Peng, J. Shi, Biomaterials 26 (2005) 5267–5275.
[21] C.H. Wang, C. Yang, Y.Y. Song, W. Gao, X.H. Xia, Adv. Funct. Mater. 15 (2005) 1267–1275.
[22] E. Laviron, J. Electroanal. Chem. 100 (1979) 263–270.
[23] S.F. Wang, T. Chen, Z.L. Zhang, X.C. Shen, Z.X. Lu, D.W. Pang, K.Y. Wong, Langmuir 21 (2005) 9260–9266.
[24] E. Laviron, J. Electroanal. Chem. 101 (1979) 19–28.
[25] Y.D. Zhao, Y.H. Bi, W.D. Zhang, Q.M. Luo, Talanta 65 (2005) 489–494.
[26] W. Sun, X.q. Li, P. Qin, K. Jiao, J. Phys. Chem. C 113 (2009) 11294–11300.
[27] A.M. Bond, Modern Polarographic Methods in Analytical Chemistry, Marcel Dekker, New York, 1980.
[28] I. Yamazaki, T. Araiso, Y. Hayashi, H. Yamada, R. Makino, Adv. Biophys. 11 (1978) 249–281.
[29] X. Ma, X.J. Liu, H. Xiao, G.X. Li, Biosens. Bioelectron. 20 (2005) 1836–1842.
[30] R.A. Kamin, G.S. Willson, Anal. Chem. 52 (1980) 1R–9R.
[31] A.H. Liu, M.D. Wei, I. Honma, H.S. Zhou, Anal. Chem. 77 (2005) 8068–8074.
[32] X.J. Zhao, Z.B. Mai, X.H. Kang, Z. Dai, X.Y. Zou, Electrochim. Acta 53 (2008) 4732–4739.
[33] X.B. Lu, H.J. Zhang, Y.W. Ni, Biosens. Bioelectron. 24 (2008) 793–798.
[34] W.L. Zhu, Y.Y. Wang, J. Xuan, J.R. Zhang, J. Nanosci. Nanotechnol. 11 (2011) 138–142.
[35] Q.L. Sheng, J.B. Zheng, X.D. Shangguan, W.H. Lin, Y.Y. Li, R.X. Liu, Electrochim. Acta 55 (2010) 3185–3191.
[36] W. Sun, P. Qin, R.J. Zhao, K. Jiao, Talanta 80 (2010) 2177–2181.
[37] H.L. Qi, C.X. Zhang, X.R. Li, Sens. Actuators B 114 (2006) 364–370.
[38] W. Sun, X.Q. Li, Y. Wang, R.J. Zhao, K. Jiao, Electrochim. Acta 54 (2009) 4141–4148.
[39] H.Y. Zhao, W. Zheng, Z.X. Meng, H.M. Zhou, X.X. Xu, Z. Li, Y.F. Zheng, Biosens. Bioelectron. 24 (2009) 2352–2357.
[40] W. Ma, D.B. Tian, Bioelectrochemistry 78 (2010) 106–112.